RSC Advances

PAPER

View Article Online
View Journal | View Issue

Cite this: *RSC Adv.*, 2025, **15**, 26444

Flavones from *Muntingia calabura* leaves: structural elucidation and SAR for α-glucosidase inhibition by *in vitro* and *in silico* evaluation†

Hai Xuan Nguyen,[abc] Thu Minh Le,[ab] Tho Huu Le,[abc] Thang Quoc Truong,[ab] Bui Quoc Huy Nguyen,[f] Phong Thanh Nguyen,[ab] Khang Minh Le,[bd] Truong Nhat Van Do,[abc] Mai Thanh Thi Nguyen,[abc] Minh Hien Nguyen *[be] and Nhan Trung Nguyen*[abc]

Phytochemical investigation of *Muntingia calabura* leaves led to the isolation of three new calaburones (**1**–**3**) and 12 known flavones (**4**–**15**). Their structures were elucidated by using advanced spectroscopic techniques and compared with existing literature. *In vitro* assay revealed that 12 out of the 15 flavones demonstrated potential α-glucosidase inhibitory activity compared to a positive control, acarbose. The three most potent compounds (**3**, **14**, and **15**), having IC_{50} values of 5.4, 12.8, and 3.1 μM, respectively, were further investigated using molecular dynamics (MD) simulations to explore the structure–activity relationship (SAR) and assess their interactions with the α-glucosidase enzyme. The SAR analysis suggests that the presence of methoxy groups at C-3 and C-8, along with a hydroxyl group at C-5, plays a crucial role in the α-glucosidase inhibitory activity of these compounds. Molecular docking and molecular dynamics (MD) simulations show that these compounds form strong interactions with key amino acids of α-glucosidase, particularly hydrogen bonds and hydrophobic interactions, leading to the structural stability of the enzyme when bound with the ligand. Compound **15** exhibits the most substantial binding with α-glucosidase, primarily through interactions at the allosteric site, enhancing the stability of the enzyme–ligand complex. These results suggest compound **15** is the most promising candidate for development as an α-glucosidase inhibitor in anti-diabetic drug discovery.

Received 14th March 2025
Accepted 17th July 2025

DOI: 10.1039/d5ra01818h

rsc.li/rsc-advances

Introduction

Diabetes mellitus is a chronic metabolic disorder characterized by persistent hyperglycemia, posing a significant global health challenge due to its rising prevalence and associated socioeconomic burden. Among various therapeutic strategies, the regulation of postprandial glucose levels plays a critical role in diabetes management. α-Glucosidase, a key carbohydrate-hydrolyzing enzyme located in the brush border of the small intestine, facilitates the breakdown of oligosaccharides into glucose. Inhibiting α-glucosidase is an established therapeutic approach that delays carbohydrate digestion and absorption, thereby mitigating postprandial hyperglycemia.[1,2] Clinically approved α-glucosidase inhibitors (AGIs), such as acarbose, voglibose, and miglitol, effectively manage type 2 diabetes mellitus (T2DM).[2,3] However, their long-term use is often associated with gastrointestinal side effects, underscoring the need for alternative inhibitors with improved efficacy and safety profiles.

Natural products have long been recognized as valuable sources of bioactive compounds for drug discovery. Among them, flavones have garnered considerable attention for their diverse pharmacological activities, including antioxidant, antiproliferative, anti-tumor, antimicrobial, antidiabetic, estrogen-like, acetylcholinesterase-inhibiting, and anti-inflammatory effects. Flavones are also applied in the treatment of cancer, cardiovascular conditions, and neurodegenerative diseases.[4] Structurally, flavones are characterized by a benzopyranone (C6–C3–C6) core, with various hydroxylation, methoxylation, and glycosylation patterns influencing their biological activity. The polypharmacological potential of flavones has been increasingly recognized, as these compounds can interact with multiple molecular targets and pathways, which may contribute

[a]*Faculty of Chemistry, University of Science, Ho Chi Minh City, Vietnam. E-mail: ntnhan@hcmus.edu.vn*
[b]*Vietnam National University, Ho Chi Minh City, Vietnam. E-mail: nmhien@uhsvnu.edu.vn*
[c]*Research Lab for Drug Discovery and Development, University of Science, Ho Chi Minh City, Vietnam*
[d]*Central Laboratory of Analysis, University of Science, Ho Chi Minh City, Vietnam*
[e]*University of Health Sciences, Vietnam National University, Ho Chi Minh City, Vietnam*
[f]*The University of Danang – VN-UK Institute for Research and Executive Education, Danang City, Vietnam*

† Electronic supplementary information (ESI) available. See DOI: https://doi.org/10.1039/d5ra01818h

to both their therapeutic efficacy and side effect profiles. While flavones are generally considered safe, the potential toxicological risks associated with chronic or high-dose exposure, particularly in the context of long-term antidiabetic therapy, should not be overlooked and warrant further investigation.[5,6] Recent studies have explored the potential of flavones as α-glucosidase inhibitors, highlighting their ability to modulate enzyme activity through specific structural features.[7] However, compared to other flavonoid subclasses such as flavonols and isoflavones, comprehensive structure–activity relationship (SAR) studies on flavone-α-glucosidase interactions remain relatively limited.

SAR investigations have revealed that specific hydroxylation and methoxylation patterns significantly impact the inhibitory potency of flavones. Hydroxyl groups at positions C-5, C-7, and C-4′ have been reported to enhance hydrogen bonding interactions with key amino acid residues in the active site of α-glucosidase, thereby increasing binding affinity.[8–10] Conversely, methoxylation or alkylation at positions C-6 or C-3′ has been associated with stronger hydrophobic interactions, which contribute to ligand stabilization within the enzyme's binding pocket.[10] Molecular docking and enzymatic assays have identified crucial amino acid residues involved in flavone binding, including Asp242, Arg315, and Glu411, with flavones primarily interacting through hydrogen bonding, electrostatic forces, and π–π stacking with aromatic residues such as Phe178 and Tyr158.[11,12] Additionally, some flavones have been suggested to bind to allosteric sites, leading to non-competitive inhibition, which may offer advantages over active-site inhibitors by reducing the risk of resistance development.[7,13]

Despite these findings, the current understanding of flavone-based α-glucosidase inhibitors remains fragmented. It is crucial that we shift our focus from isolated flavone derivatives to establishing a comprehensive SAR framework. Furthermore, while *in vitro* enzyme inhibition assays are widely employed, *in silico* molecular modeling and *in vivo* validation remain underdeveloped, limiting the translational potential of these compounds. The lack of systematic evaluation of flavone derivatives across diverse structural modifications further hampers the rational design of more potent and selective inhibitors. To advance this field, future studies should prioritize expanding SAR analysis by incorporating a broader range of flavone analogs, employing molecular dynamics simulations to assess binding stability, and validating promising inhibitors through preclinical and clinical studies. Given the increasing global burden of diabetes and the demand for safer, more effective therapeutic options, flavone-based α-glucosidase inhibitors represent a promising yet underexplored avenue in drug discovery.

Muntingia calabura L. (*Muntingiaceae*), commonly known as "Trứng cá" in Vietnam, is a tropical plant widely used in traditional medicine for treating diabetes, inflammation, and bacterial infections.[14] Phytochemical studies have revealed that the plant is rich in tocopherols, flavonoids, chalcones, and sterols. In our previous study, we identified six δ-tocopherol derivatives, four flavonoids, and five steroids from the ethyl acetate extract of *M. calabura* leaves, in which there was a newly described trimeric δ-tocopherol derivative.[15–20] Moreover, flavones are a dominant component of the flavonoid content, which has led to increasing interest in their bioactive potential. While extracts from *M. calabura* have shown promise for their antioxidant, anti-inflammatory, antidiabetic, and antimicrobial properties, their ability to inhibit α-glucosidase, a key enzyme involved in glucose metabolism, has yet to be comprehensively studied.[21,22]

Therefore, this study identifies and evaluates the α-glucosidase inhibitory potential of flavones isolated from *M. calabura* leaves through a combination of experimental and computational approaches. This study led to the isolation of three new flavones, calaburone A (**1**), calaburone B (**2**), and calaburone C (**3**), along with 12 known flavones (**4–15**). The objectives include isolating flavones, determining their chemical structures, and assessing their α-glucosidase inhibitory activities to elucidate the role of structural features in modulating bioactivity. Additionally, *in silico* docking and binding energy calculations will be performed to explore interactions between the flavones and the active site of α-glucosidase, identifying key binding motifs and energetically favorable conformations. The findings of this study will not only deepen our understanding of the structural basis of α-glucosidase inhibition by flavones but also position *M. calabura* as a promising natural source of antidiabetic agents. By integrating *in vitro* and *in silico* approaches, this study aims to identify novel α-glucosidase inhibitors from natural product sources.

Results and discussion

The dried leaves of *M. calabura* L. were subjected to sequential extraction with *n*-hexane, ethyl acetate (EtOAc), and methanol (MeOH) using a Soxhlet extraction system, yielding *n*-hexane, EtOAc, and MeOH extracts. Through a combination of chromatographic methods, including normal-phase silica gel, RP-18 silica gel, and preparative thin-layer chromatography (TLC), three novel compounds (**1–3**) and twelve previously known compounds (**4–15**) (Fig. 1) were successfully isolated from the EtOAc extract. The previously identified compounds were characterized as 7-hydroxyflavone (**4**),[23] 7-hydroxy-8-methoxyflavone (**5**),[24] 3,7-dimethoxyflavone (**6**),[25] 5,7-dimethoxy-6-hydroxyflavone (**7**),[26] kaempferol (**8**),[27] 4′-hydroxywogonin (**9**),[28] 6,7-dimethoxy-5,4′-dihydroxyflavone (**10**),[29] 5-hydroxy-7,4′-dimethoxyflavone (**11**),[30,31] 7-hydroxy-4′-methoxyflavone (**12**),[32] quercetin 3,7-dimethyl ether (**13**),[33] quercetin 3,3′-dimethyl ether (**14**)[34] and 5,7,4′-trihydroxy-3,8-dimethoxyflavone (**15**).[35]

Compound **1** was isolated as a yellowish amorphous solid. The compound showed a pseudo-molecular ion at *m*/*z* 329.1035 $[M + H]^+$, corresponding to the empirical formula $C_{18}H_{17}O_6^+$ (calculated for 329.1025), thereby confirming the molecular formula as $C_{18}H_{16}O_6$ in HR-ESI-MS. The IR spectra showed absorption bands at 3458 cm^{-1} (stretching of O–H), 2925 cm^{-1} (stretching of C–H), 1737 cm^{-1} (stretching of C=O), 1509 cm^{-1} (stretching of C=C), 1366 cm^{-1} (bending of O–H), 1104 cm^{-1} (bending of C–O), and 702 cm^{-1} (bending of C–H). The ^{1}H-NMR spectrum displayed signals of five aromatic protons [δ_H 8.14–

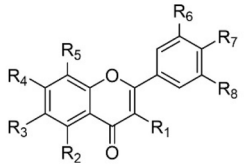

	R_1	R_2	R_3	R_4	R_5	R_6	R_7	R_8
1	OCH_3	H	OCH_3	OCH_3	OH	H	H	H
2	H	H	H	OH	OCH_3	OH	OCH_3	OCH_3
3	OCH_3	OH	H	OH	OCH_3	OH	H	H
4	H	H	H	OH	H	H	H	H
5	H	H	H	OH	OCH_3	H	H	H
6	OCH_3	H	H	OCH_3	H	H	H	H
7	H	OCH_3	OH	OCH_3	H	H	H	H
8	OH	OH	H	OH	H	H	OH	H
9	H	OH	H	OH	OCH_3	H	OH	H
10	H	OH	OCH_3	OCH_3	H	H	OH	H
11	H	OH	H	OCH_3	H	H	OCH_3	H
12	H	H	H	OH	H	H	OCH_3	H
13	OCH_3	OH	H	OCH_3	H	OH	OH	H
14	OCH_3	OH	H	OH	H	OCH_3	OH	H
15	OCH_3	OH	H	OH	OCH_3	H	OH	H

Fig. 1 Structures of three new flavones (**1–3**) together with twelve known flavones (**4–15**) isolated from *M. calabura* L. leaves.

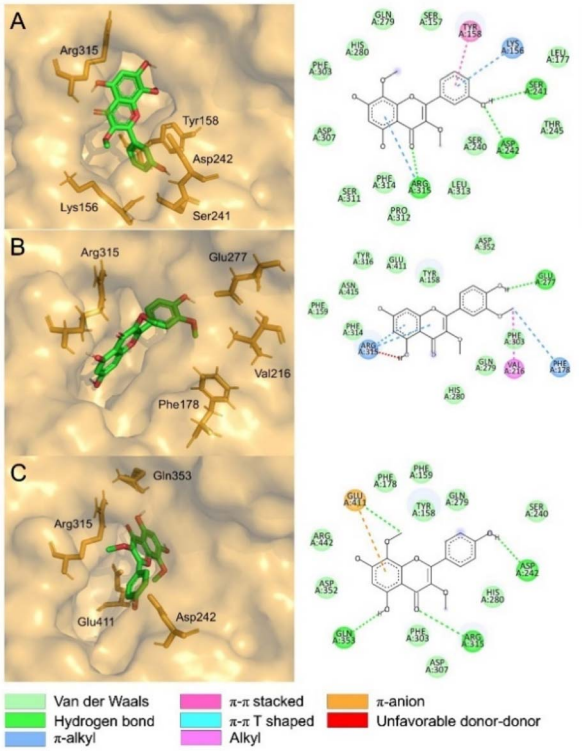

Fig. 3 Binding poses and 2D interactions between the α-glucosidase and compound **3** (A), compound **14** (B), and compound **15** (C).

7.56 (5H; m; H-2′, H-3′, H-4′, H-5′, H-6′)] corresponding to the mono-substituted benzene and one isolated aromatic proton [δ_H 6.50 (1H; s; H-5)], together with three methoxyl groups [δ_H 3.92–3.85 (9H; s; 3-OCH_3, 6-OCH_3, 7-OCH_3)] and a free hydroxyl group [δ_H 9.19 (1H; s; 8-OH)]. Additionally, the ^{13}C-NMR and DEPT spectra revealed the signals of a ketone carbonyl carbon [δ_C 172.5 (C-4)], two oxygenated olefinic carbons [δ_C 151.5 (C-2), 141.4 (C-3)], twelve aromatic carbons [δ_C 96.0 (C-5), 156.4 (C-6), 128.8 (C-7), 154.6 (C-8), 151.2 (C-9), 108.8 (C-10), 131.3, (C-1′), 127.9 (C-2′, C-6′), 128.6 (C-3′, C-5′), 130.2 (C-4′)], and three methoxyl carbons [δ_C 59.1 (3-OCH_3), 55.6 (6-OCH_3), 60.9 (7-OCH_3)]. The compound was thus a tetra-oxygenated flavone having a hydroxyl and three methoxyl groups. In the ^{1}H–^{1}H COSY and HSQC spectra, the B-benzene ring was determined as the mono-substituted benzene because of the bold lines in the Fig. 2 forming the segment C(1′)–C(2′)H–C(3′)H–C(4′)H–C(5′)H–C(6′)H. In the HMBC spectrum, the isolated aromatic proton at δ_H 6.50 correlated to the carbonyl carbon (C-4) and three aromatic carbons (C-6, C-7, C-10) showed that it was affixed to the C-5 of the flavone skeleton. The location of two of three methoxyl groups at C-6 and C-7 is based on the HMBC correlations of the methoxyl proton at δ_H 3.85 with δ_C 156.4 (C-6) and of the methoxyl proton at δ_H 3.92 with δ_C 128.8 (C-7), higher magnetic field, as being between two oxygenated aromatic carbons C-6 and C-8. Meanwhile, the HMBC spectrum also presented the interactions from the free hydroxyl proton at δ_H 9.19 to two aromatic carbons (C-7, C-8), affirming that C-8 bears a hydroxyl group. The remaining methoxyl group was attached to the C-3 due to the HMBC correlation between the methoxyl protons with an oxygenated aromatic carbon (C-3). Two adjacent methoxyl groups were confirmed by the NOE correlation in Fig. 2. Compound **1** was, therefore, an 8-hydroxy-3,6,7-trimethoxyflavone named calaburone A.

Compound **2** was obtained as a yellowish amorphous solid. Its HR-ESI-MS showed a pseudo-molecular ion at *m*/*z* 345.0990 $[M + H]^+$ (calcd for 345.0974), corresponding to the molecular formula $C_{18}H_{16}O_7$. The IR spectrum of **2** indicated absorptions

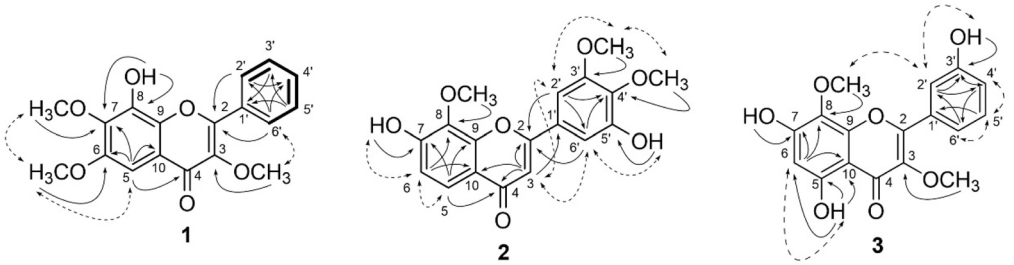

Fig. 2 The key HMBC (solid arrows) and NOESY (dashed arrows) correlations of three new calaburones A–C (**1–3**).

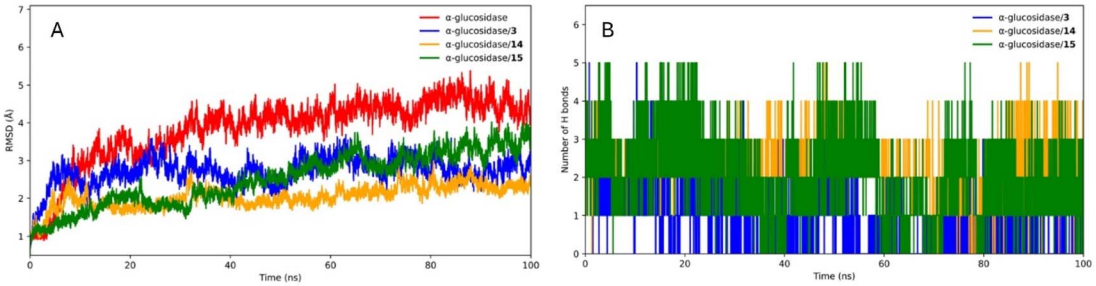

Fig. 4 MD simulation of RMSD (A) and hydrogen bond number (B) over times of α-glucosidase with calaburone C (α-glucosidase/**3**; blue), quercetin 3,3′-dimethyl ether (α-glucosidase/**14**; orange), 5,7,4′-trihydroxy-3,8-dimethoxyflavone (α-glucosidase/**15**; green), and without binding (α-glucosidase; red).

of hydroxyl (3358, 1377 cm^{-1}), ketone carbonyl (1723, 1107 cm^{-1}), and benzene (1626, 1510, 1454 cm^{-1}) groups. The ^{1}H and ^{13}C NMR spectra of **2** exhibited signals of a flavone unit consisting of an isolated olefinic proton [δ_H 6.71 (1H; s; H-3) and δ_C 106.2 (C-3)], a conjugated carbonyl carbon [δ_C 176.5 (C-4)], a 1,2,3,4-tetrasubstituted A-benzene ring [δ_H 7.73 (1H, d, J = 8.8 Hz, H-5), 7.03 (1H, t, J = 8.8 Hz, H-6) and δ_C 120.5 (C-5), 114.4 (C-6), 154.7 (C-7), 135.3 (C-8), 150.7 (C9), 118.8 (C10)], a 1,3,4,5-tetrasubstituted B-benzene ring [δ_H 7.24 (1H, d, J = 2.2 Hz, H-2′), 7.27 (1H, d, J = 2.2 Hz, H-6′) and δ_C 128.0 (C-1′), 101.9 (C-2′), 153.7 (C-3′), 139.3 (C-4′), 151.0 (C-5′), 107.1 (C-6′)], along with three methoxyl groups [δ_H 4.08 (3H; s; 8-OCH_3), 4.00 (3H; s; 3′-OCH_3), 3.87 (3H; s; 4′-OCH_3) and δ_C 61.1 (8-OCH_3), 55.6 (3′-OCH_3), 60.0 (4′-OCH_3)] and two free hydroxyl groups [δ_H 9.24 (1H; s; 7-OH), 8.39 (1H; s; 5′-OH)]. In the HMBC spectrum (Fig. 2), the isolated olefinic proton (H-3) displayed cross-peaks with the carbonyl carbon (C-4) and two substituted aromatic carbons (C-10, C-1′).

Two *meta*-coupled aromatic protons (H-2′, H-6′) correlated to the oxygenated olefinic carbon (C-2), indicating that the 1,3,4,5-tetrasubstituted B-benzene ring was attached to the C-2. There had the hydroxyl group (δ_H 8.39) at C-5′ based on the HMBC correlation from it to the oxygenated aromatic carbon (δ_C 151.0), and two methoxyl groups at C-3′ and C-4′ which was higher shielding field than that of C-3′ since the carbone C-4′ was between two oxygenated aromatic carbons C-3′ and C-5′. This was supported by the NOE correlation in Fig. 2. One of the two *ortho*-coupled aromatic protons (H-5) correlated to the carbonyl carbon (C-4), and the other correlated to the substituted aromatic carbon (C-10). The other hydroxyl group was C-7, and the other methoxyl group was C-8, with stronger field magnetic resonance because of their HMBC correlations. The compound **2** was hence a 7,5′-dihydroxy-8,3′,4′-trimethoxyflavone, which was named calaburone B.

Compound **3** was obtained as a yellowish amorphous solid with the molecular formula $C_{17}H_{14}O_7$, as determined by HR-ESI-MS. The IR spectrum of **3** illustrates absorptions of hydroxyl (3420, 1314 cm^{-1}), ketone carbonyl (1648, 1081 cm^{-1}), and benzene (1599, 1514, 1455 cm^{-1}) groups. The ^{1}H- and ^{13}C-NMR spectra showed that a part of these data closely resembled those for 5,7,4′-trihydroxy-3,8-dimethoxyflavone (**15**)[35] and indicated the presence of a flavone skeleton with a chelated hydroxyl, two free hydroxyl groups, and two methoxyl groups. However, it appeared signals for a 1,3-disubstituted B-benzene ring [δ_H 7.66 (1H, t, J = 2.5 Hz, H-2′), 7.64 (1H, dt, J = 8.0 & 2.5 Hz, H-4′), 7.41 (1H, t, J = 8.0 Hz, H-5′), 7.05 (1H, dt, J = 8.0 & 2.5 Hz, H-6′) and

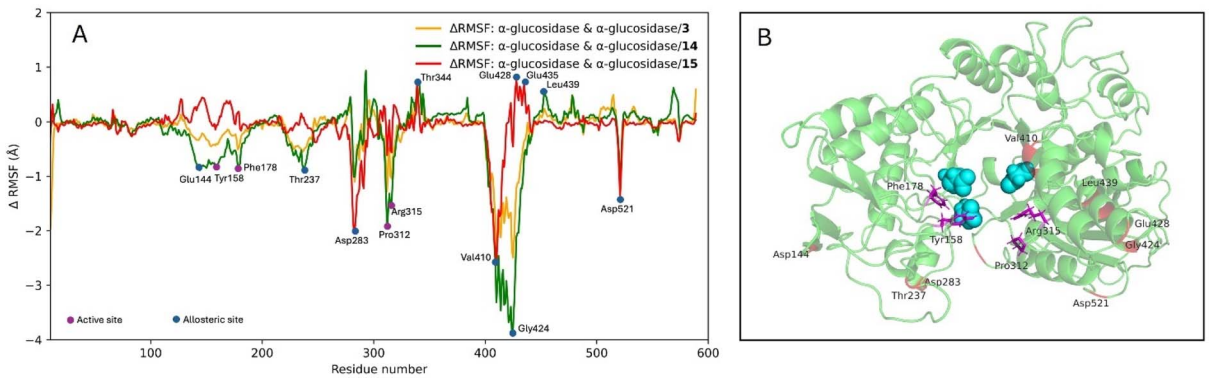

Fig. 5 MD simulation of ΔRMSF (A) over amino acid residues of α-glucosidase with calaburone C (α-glucosidase/**3**; orange), quercetin 3,3′-dimethyl ether (α-glucosidase/**14**; green), 5,7,4′-trihydroxy-3,8-dimethoxyflavone (α-glucosidase/**15**; red). Negative values indicate a decrease in the fluctuation of amino acid residue, while the positive ones exhibit an increase. The 3D structure of α-glucosidase (B) is presented in a close-up view. The active sites are represented in spheres, and other amino acids at the binding pocket are illustrated as magenta sticks. Amino acids in the allosteric site are labeled in red.

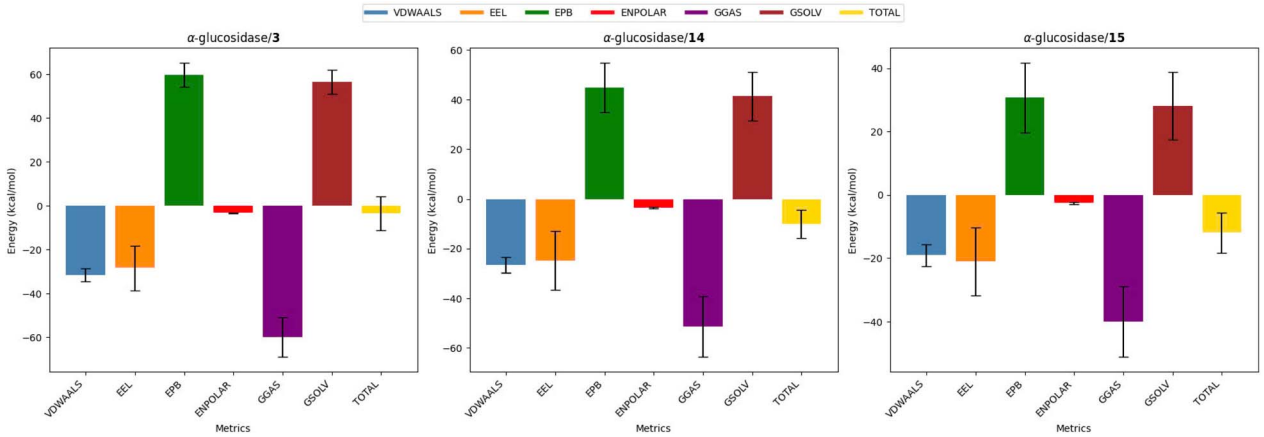

Fig. 6 The binding free energy of compounds **3**, **14**, and **15** was calculated using the MMPBSA method.

δ_C 131.9 (C-1′), 115.0 (C-2′), 155.3 (C-3′), 119.5 (C-4′), 129.8 (C-5′), 118.1 (C-6′)] in **3** and disappeared signals for a 1,4-disubstituted B-benzene ring in **15**. From the HMBC experiment, a free hydroxyl group [δ_H 8.99 (1H; s; 3′-OH)] showed a cross-peak with an O-bearing aromatic carbon [δ_C 155.3 (C-3′)], which is a lower shielding field. The compound **3** was consequently a 5,7,3′-trihydroxy-8,3′-dimethoxyflavone, which was named calaburone C.

The α-glucosidase inhibitory activity[36] of the isolated compounds was evaluated with an assay performed at concentrations ranging from 10 to 250 μM. The result showed that 14 out of 15 compounds were able to inhibit more than 50% of the enzyme at 250 μM, and 12 of them displayed an inhibition rate greater than 50% at 100 μM. Notably, compounds **3** and **15** were found to be inhibitory over 50% at 10 μM, so they continued to be tested for the α-glucosidase inhibitory assay at five lower concentrations, ranging from 25–1 μM. In Table 2, except for compounds **4** and **11**, the other compounds demonstrated greater potency than that of a positive control, acarbose (IC_{50}; 185.2 μM), which is currently used

Table 1 The ^{1}H- and ^{13}C-NMR data of compounds **1–3** in CD_3COCD_3

	1		**2**		**3**	
Position	δ_H (J in Hz)	δ_C, type	δ_H (J in Hz)	δ_C, type	δ_H (J in Hz)	δ_C, type
2		151.5, C		162.1, C		157.6, C
3		141.4, C	6.71, s	106.2, CH		139.4, C
4		172.5, C		176.5, C		179.0, C
5	6.50, s	96.1, CH	7.73, d (8.8)	120.5, CH		157.1, C
6		156.4, C	7.03, d (8.8)	114.4, CH	6.32, s	98.7, CH
7		128.8, C		154.7, C		156.9, C
8		154.6, C		135.3, C		127.7, C
9		151.2, C		150.7, C		149.0, C
10		108.8, C		118.8, C		105.1, C
1′		131.3, C		128.0, C		131.9, C
2′	8.14–8.11, m	127.9, CH	7.24, d (2.2)	101.9, CH	7.66, t (2.5)	115.0, CH
3′	7.56–7.51, m	128.6, CH		153.7, C		155.3, C
4′	7.59–7.57, m	130.2, CH		139.3, C	7.64, dt (8.0, 2.5)	119.5, CH
5′	7.56–7.51, m	128.6, CH		151.0, C	7.41, t (8.0)	129.8, CH
6′	8.14–8.11, m	127.9, CH	7.27, d (2.2)	107.1, C	7.05, dt (8.0, 2.5)	118.1, CH
3-OCH_3	3.86, s	59.1, CH_3			3.89, s	59.6, CH_3
6-OCH_3	3.85, s	55.6, CH_3				
7-OCH_3	3.92, s	60.9, CH_3				
8-OCH_3			4.08, s	61.1, CH_3	3.91, s	61.0, CH_3
3′-OCH_3			4.00, s	55.6, CH_3		
4′-OCH_3			3.87, s	60.0, CH_3		
5-OH					12.37, s	
7-OH			9.24, s		9.62, s	
8-OH	9.19, s					
3′-OH					8.99, s	
5′-OH			8.39, s			

Table 2 α-Glucosidase inhibitory activity of all isolated compounds[a]

Compounds	Inhibition (*I*, %) 250 μM	100 μM	50 μM	25 μM	10 μM	IC_{50} (μM)
1	[b]	96.8 ± 2.5	49.1 ± 1.9	20.4 ± 2.7	8.2 ± 3.0	52.8
2	[b]	98.7 ± 1.0	72.6 ± 4.4	20.0 ± 2.4	3.0 ± 1.7	39.2
4	37.1 ± 1.2	7.2 ± 3.5	[c]	[c]	[c]	>250
5	[b]	89.3 ± 2.8	42.7 ± 2.7	6.5 ± 1.9	[c]	61.9
6	[b]	91.7 ± 3.8	23.24 ± 1.7	11.5 ± 3.0	[c]	42.9
7	98.4 ± 3.8	69.6 ± 2.1	21.15 ± 1.5	7.09 ± 4.3	[c]	78.7
8	[b]	98.5 ± 2.2	84.9 ± 1.1	44.1 ± 2.9	8.6 ± 1.4	28.6
9	[b]	[b]	94.9 ± 2.6	58.2 ± 1.3	20.5 ± 4.2	19.5
10	[b]	97.5 ± 1.0	86.64 ± 1.8	45.1 ± 2.2	23.4 ± 1.2	22.8
11	52.0 ± 1.4	15.7 ± 2.4	3.7 ± 2.6	[c]	[c]	244.8
12	85.1 ± 2.7	34.4 ± 1.7	16.3 ± 2.9	7.4 ± 1.0	[c]	143.6
13	86.4 ± 1.2	50.1 ± 1.5	23.4 ± 3.3	14.2 ± 3.6	5.9 ± 4.8	~100
14	[b]	96.8 ± 1.3	94.91 ± 1.4	69.3 ± 3.2	43.1 ± 1.8	12.8
Acarbose[d]	63.8 ± 1.0	26.8 ± 1.0	21.0 ± 1.6	9.3 ± 1.2	5.45 ± 0.68	185.2

Compounds	Inhibition (*I*, %) 25 μM	10 μM	5 μM	2.5 μM	1 μM	IC_{50} (μM)
3	92.2 ± 1.6	74.9 ± 1.5	47.0 ± 2.4	20.2 ± 1.2	6.8 ± 2.0	5.4
15	96.3 ± 1.2	82.5 ± 0.8	62.1 ± 2.9	40.1 ± 2.1	24.7 ± 1.4	3.1

[a] IC_{50} results are expressed as the average of three independent replicates. A *p*-value less than 0.05 was considered statistically significant. [b] Inhibition > 99%. [c] Inhibition < 1%. [d] Positive control.

clinically in combination with either diet or anti-diabetic agents to control the blood glucose levels of patients.[37] Significantly, the new calaburone C (**3**) and 5,7,4′-trihydroxy-3,8-dimethoxyflavone (**15**) have been the most active compounds with their IC_{50} values of 5.4 and 3.1 μM, respectively.

The α-glucosidase inhibitory activity of these compounds was dependent upon the nature of the substitution, and careful evaluation of the IC_{50} values led to the correlation between structure and activity. Firstly, all of the 3-methoxylated flavones had stronger activity with IC_{50} values lower than 43 μM. For example, the inhibitory activity of 5,7,4′-trihydroxy-3,8-dimethoxyflavone (**15**; IC_{50} = 3.1 μM) was more potent than that of 4′-hydroxywogonin (**9**; IC_{50} = 19.5 μM). Additionally, a methoxyl group at C-8 of flavones played a crucial role in vigorous α-glucosidase inhibitory activity (**5** ≫ **4**). Finally, compounds **3**, **8–10**, **14**, and **15**, which were a chelated hydroxyl group at C-5, had their IC_{50} values lower than 30 μM, indicating it being a stronger activity than those without substituent at the same position. These results proved that the most vigorous activity of compounds **3** and **15** might be attributable to the presence of two methoxyl groups at C-3 and C-8 and a hydroxyl group at C-5. Besides, the presence of the methoxyl group at C-4′ was highly essential for the α-glucosidase inhibitory activity (**12** > **4**). While these *in vitro* results provide valuable insights into the α-glucosidase inhibitory activity of the compounds, molecular docking and dynamics simulations were employed to further elucidate the binding interactions and provide a structural basis for the observed activity.

Compounds **3**, **14**, and **15**, with the highest values of IC_{50}, were subjected to molecular docking and molecular dynamics (MD) simulation to give insights into the molecular interactions between ligands and enzyme α-glucosidase. Three compounds

Table 3 Binding energy and interactions between key amino acids of the α-glucosidase and compounds **3**, **14**, and **15**

Compounds	Binding energy (kcal mol^{-1})	Residue interactions
3	−8.4	H-bond: Ser241 (2.2 Å), Asp242 (3.3 Å), Arg315 (2.8 Å) π–π stacked: Tyr158 (4.3 Å) π-alkyl: Lys156 (4.2 Å), Arg315 (4.0 Å)
14	−8.1	H-bond: Glu277 (2.1 Å) Alkyl: Val216 (3.3 Å) π-alkyl: Phe178 (2.8 Å), Arg315 (3.5 Å) Unfavorable donor–donor: Arg315 (1.7 Å)
15	−8.2	H-bond: Asp242 (2.9 Å), Arg315 (3.1 Å), Gln353 (2.1 Å), Glu411 (3.8 Å) π-anion: Glu411 (4.5 Å)

docked at the active site of the α-glucosidase exhibit a strong binding energy, more than 8.0 kcal mol^{-1} (Table 3). As shown in Fig. 3, these three compounds adopt the L-shape conformation in the binding pocket, forming key interactions with the catalytic residues, including Glu277, Gln353, and Tyr158. These residues, located at the C-terminal of a barrel in domain A (residues 1–113 and 190–512), plays a crucial role in the enzymatic activity of α-glucosidase by facilitating the binding of the substrate and the subsequent catalysis.[38] Additional hydrogen bonds between the carbonyl oxygens of the flavone ring with Asp242 and Arg315 highlight the binding affinities of the compounds **3** and **15** bound to α-glucosidase. Notably, compound **3** binds to a unique allosteric site, forming two hydrogen bonds between Ser241 (2.2 Å), Asp242 (3.3 Å), and the hydroxyl group of the phenyl ring. Hydrophobic interactions were also observed between Val216 and Phe178 and the methoxy group of the phenyl ring in compound **14**. Electrostatic interaction was illustrated between the benzopyranone ring of compound **15** and the Glu411 amino acid residue.

In addition to molecular docking, we employed molecular dynamics (MD) simulations to further evaluate the stability and behavior of the ligand–protein complexes under near-physiological conditions. Unlike docking, which assumes a static binding mode, MD simulations incorporate the dynamic nature of both the ligand and the protein, thereby addressing a major limitation of rigid docking. The results obtained from root mean square deviation (RMSD) and root mean square fluctuation (RMSF) analyses provided valuable insights into the structural stability and flexibility of the complexes over time. Consequently, MD simulations allow for the prioritization of compounds by filtering out unstable or weakly interacting complexes, thereby increasing the reliability of computational predictions prior to costly *in vitro* and *in vivo* validation. Multiple MD simulations for free and ligand-bound enzymes were performed during 100 ns to assess the structural stability. The structural analysis of these trajectories revealed that the RMSD values decreased almost half from 4.0–4.5 Å in the ligand-free to 2.0–2.5 Å in compounds **14** and **3**-bound enzyme structures, respectively, and these structures stabilized after 60 ns of simulation. In the case of compound **15**, the RMSD values are below 3.0 Å during simulation time with slight fluctuation. In summary, these RMSD patterns reveal that ligand-bound enzyme structures are more stable than the free enzyme. Aligning with the molecular docking analysis and RMSD results, the hydrogen numbers of ligand-bound enzymes are highest (3–5 hydrogen bonds) for α-glucosidase/**15** complex and lowest (2–3 hydrogen bonds) for α-glucosidase/**3** complex. Compound **14** bound α-glucosidase reaches a stable state only after 35 ns (Fig. 4A). Meanwhile, hydrogen bond numbers increase after this period (Fig. 4B). The RMSF analysis was carried out to assess the fluctuation of individual amino acid residues.

Accompanying the docking and RMSD analysis, the MD simulation of ΔRMSF results reveal the mixed nature of inhibition of these three compounds as competitive or uncompetitive inhibitors. In general, the negative peaks at Tyr158, Phe178, Pro312, and Arg315 were observed for all three compounds, showing a decrease in the residue fluctuation due to the rigidity after forming the ligand-bound enzyme. As in the previous study, Tyr158, His280, and loop 310–315 are located at the entrance of the active site pocket; therefore, their mobility enables the substrate to enter the active site.[38] However, loop 310–315 is not highly flexible enough to be considered an entrance exit for the release of products in a "trap-release" mechanism. Interestingly, some other residues exhibit high positive variations, including Ser344, Tyr347, and Leu439, that are in a turn, a turn, and an α helix secondary structures, respectively; in other meaning, the formation of complex enhances the mobility of the residues.

Furthermore, the significant difference in the fluctuation of amino acids Thr237, Asp283, and Val410–Gly424, which are in a loop, a turn, and an α helix in domain A (as shown in red in Fig. 5B), is observed, demonstrating the importance of the allosteric site in binding affinity. To support this hypothesis, as can be seen in Fig. 2, the differences in RMSF values of amino acids at the active site are conversely with those of amino acids at the allosteric site. Compounds **15** show a significant effect of the allosteric site compared with binding the active site, while compounds **3** and **14** are affected less by the allosteric site. These results are consistent with the nature of allosteric sites as they indirectly affect the active site.[39]

The Molecular Mechanics Poisson-Boltzmann Surface Area (MMPBSA) method was applied to estimate the binding free energy of three compounds, as shown in Fig. 6. van der Waals interactions (VDWAALS) and electrostatic interactions (EEL) were identified as the main contributors to the gas phase energy (GGAS), while GSOLV was the total of polar (EPB) and nonpolar (ENPOLAR) interactions. For each system, the total free energy was the sum of the gas phase energy (GGAS) and the solvation energy (GSOL). EMPOLAR interactions, with the lowest values, were found to be indistinguishable from EEL interactions among the three ligands, with an approximate value of −3 kcal mol^{-1}. van der Waals interactions varied among the ligands, with the most significant contribution observed in the case of compound **3**, with a value of −31.53 kcal mol^{-1}. The ratio between GGAS and GSOL was found to be conversed between compound **3** and compounds **14** and **15**, resulting in the highest binding free energy of compound **15** bound enzyme with −11.92 kcal mol^{-1}, followed by compound **14** with −10.03 kcal mol^{-1} and the lowest one of compound **3** bound enzyme with −3.48 kcal mol^{-1}.

Combining the analysis of RMSD, hydrogen bond number, RMSF, and free binding energy of the top three compounds, compound **15** demonstrated the most favorable binding with α-glucosidase. The predominance of the nonpolar interactions in compound **3**, **14** is also consistent with a hydrophobic binding cavity in the molecular docking step and underscores the importance of the allosteric site. Accompanying the docking and RMSD analysis, the MD simulation of ΔRMSF results reveals the mixed nature of inhibition of these three compounds as competitive or uncompetitive inhibitors. In general, the negative peaks at Tyr158, Phe178, Pro312, and Arg315 were observed for all three compounds, showing a decrease in the residue fluctuation due to the rigidity after

forming the ligand-bound enzyme. As in the previous study, Tyr158, His280, and loop 310–315 are located at the entrance of the active site pocket; therefore, their mobility enables the substrate to enter the active site.[38] However, loop 310–315 is not highly flexible enough to be considered an entrance exit for the release of products in a "trap-release" mechanism.

Conclusion

In conclusion, three new flavones (**1–3**) and 12 known compounds (**4–15**) were isolated from the EtOAc extract of *Muntingia calabura* L. leaves. Among them, 12 flavones (**1–3**, **5–10**, **13–15**) showed significant α-glucosidase inhibitory activity, outperforming acarbose. Notably, compounds **3**, **14**, and **15** exhibited the strongest inhibition, with compound **15** showing the lowest IC_{50} (3.1 μM). SAR analysis indicated that methoxyl groups at C-3 and C-8 and a hydroxyl at C-5 enhance activity. While limited by the number of isolated flavones, molecular docking and MD simulations confirmed strong and stable interactions with key α-glucosidase residues, especially for compound **15** at the allosteric site. These results suggest compound **15** as a promising α-glucosidase inhibitor. However, further *in vitro* and *in vivo* studies are required to determine their therapeutic window and minimize unintended interactions with non-target proteins or cell types.

Experimental section

Instruments

Multiple experimental techniques were utilized to gather comprehensive analytical data. Optical rotations were determined using an A.KRÜSS Optronic P8000 polarimeter. Infrared (IR) spectra were obtained using a JASCO FT/IR-6600 spectrometer from JASCO International Co., Ltd. Ultraviolet (UV) spectra were measured with a Shimadzu UV-1800 spectrophotometer from Shimadzu Pte., Ltd. Nuclear Magnetic Resonance (NMR) spectra were recorded on a Bruker Avance III 500 spectrometer (Bruker BioSpin AG), employing deuterated solvents as internal references, with chemical shifts noted as δ values. High-resolution electrospray ionization mass spectrometry (HR-ESI-MS) was conducted using an Xevo G2-XS QTOF Mass Spectrometer supplied by Waters and an X500R QTOF supplied by Sciex. Column chromatography was performed with silica gel 60 (0.06–0.2 mm, Scharlau, Barcelona, Spain) and LiChroprep RP-18 (40–63 μm, Merck KGaA, Darmstadt, Germany). Thin-layer chromatography (TLC) was conducted using Kieselgel 60 F254 or RP-18 F254 plates from Merck (Merck KGaA, Darmstadt, Germany).

Chemicals

Enzyme α-glucosidase from *Saccharomyces cerevisiae* and *p*-nitrophenyl-α-D-glucopyranoside were sourced from Sigma-Aldrich Pte. Ltd. Acarbose, Na_2CO_3, and DMSO from Merck were used for analysis. All other chemicals were of the highest available purity.

Plant materials

The leaves of *Muntingia calabura* L. were collected in May 2017 from Ho Chi Minh City, Vietnam. The plant's botanical identification was verified by Dr Anh Tuan Dang-Le from the Faculty of Biology and Biotechnology at the University of Science, Ho Chi Minh City, Vietnam. A voucher specimen (MDC-9002) has been properly archived in the Department of Medicinal Chemistry, Faculty of Chemistry, University of Science, Ho Chi Minh City, Vietnam.

Extraction and isolation

From 3.0 kg of dried *Muntingia calabura* leaves, the material was cut into small pieces and sequentially extracted using a Soxhlet apparatus with solvents of increasing polarity: *n*-hexane, ethyl acetate, and methanol. The extracts were concentrated under reduced pressure to recover the solvents, yielding crude extracts of *n*-hexane (143.8 g), ethyl acetate (139.1 g), and methanol (286.0 g). The ethyl acetate extract (139.1 g) was subjected to normal-phase column chromatography using a gradient elution system of acetone–*n*-hexane (v/v, 0 : 100 → 100 : 0), resulting in 13 fractions designated as **A** (15.7 g), **B** (9.2 g), **C** (1.4 g), **D** (3.0 g), **E** (447.5 mg), **F** (2.5 g), **G** (2.8 g), **H** (9.7 g), **I** (7.2 g), **J** (3.2 g), **K** (2.7 g), **L** (30.2 g), and **M** (17.9 g).

Fraction **G** (2.8 g) was subjected to silica gel column chromatography using acetone–*n*-hexane mixtures (v/v, 0 : 100 → 100 : 0) as the eluent, resulting in the separation into twelve subfractions (**G1–G12**). Subfraction **G4** (239.8 mg) was further purified through silica gel column chromatography and eluted with acetone–*n*-hexane mixtures (v/v, 0 : 100 → 100 : 0), yielding five subfractions (**G4.1–G4.5**). Subfraction **G4.2** was purified by normal phase preparative TLC with a $CHCl_3$–*n*-hexane mixture (v/v, 20 : 80) to furnish **6** (1.7 mg) and **11** (6.7 mg).

Fraction **J** (3.2 g) was applied to a silica gel column and eluted with acetone–$CHCl_3$ mixtures (v/v, 0 : 100 → 40 : 60) to yield nine fractions (**J1–J9**). Fraction **J2** (43.0 mg) was submitted to a silica gel column chromatography and eluted with acetone–*n*-hexane mixtures (v/v, 0 : 100 → 100 : 0), and then followed by normal-phase preparative TLC with ethyl acetate–*n*-hexane mixture (v/v, 30 : 70) to give **5** (10.0 mg). Fraction **J4** (272.5 mg) was loaded onto a silica gel column and eluted with EtOAc–*n*-hexane mixtures (v/v, 0 : 100 → 100 : 0) to yield four subfractions (**J4.1–J4.4**). Subfraction **J4.3** was chromatographed on silica gel with MeOH–$CHCl_3$ mixtures (v/v, 0 : 100 → 60 : 40), and the resulting fractions were purified by normal phase preparative TLC with a MeOH–$CHCl_3$ mixture (v/v, 5 : 95) to furnish **4** (9.8 mg).

Fraction **K** (2.7 g) was passed over a silica gel column chromatography, eluted with acetone–$CHCl_3$ gradient mixtures (v/v, 0 : 100 → 70 : 30), to yield 10 subfractions (**K1–K10**). Subfraction **K4** (350.7 mg) was chromatographed over a silica gel column, eluted with acetone–*n*-hexane gradient mixtures (v/v, 0 : 100 → 100 : 0), to give six subfractions (**K4.1–K4.6**). Subfraction **K4.5** (24.7 mg) was recrystallized using $CHCl_3$ as the solvent and further purified through preparative thin-layer chromatography with an ethyl acetate–$CHCl_3$ mixture (v/v, 20 : 80) elution solvent system to obtain **10** (9.0 mg). Subfraction **K5** (1.4 g) was

separated by column chromatography and eluted with acetone–*n*-hexane gradient mixtures (v/v, 0 : 100 → 100 : 0) to yield five subfractions (**K5.1–K5.5**). Subfractions **K5.2** (499.7 mg) were subjected to further silica gel column chromatography. It was eluted with acetone–*n*-hexane (v/v, 0 : 100 → 100 : 0) mixtures to yield ten subfractions (**K5.2.1–K5.2.10**) and subfraction **K5.2.4** (46.9 mg) then purified by preparative normal-phase TLC eluted with MeOH–$CHCl_3$ mixture (v/v, 6 : 94) to afford **14** (5.1 mg). Subfraction **K5.2.7** (99.9 mg) was again chromatographed with isopropanol–*n*-hexane (v/v, 0 : 100 → 70 : 30) and then purified by preparative TLC with isopropanol–ethyl acetate–$CHCl_3$ (2 : 8 : 90) to afford **3** (3.2 mg) and by preparative TLC with methanol–$CHCl_3$–*n*-hexane (5 : 55 : 40) to obtain **15** (4.3 mg). Subfraction **K5.4** (121.2 mg) was subjected to passage over a silica gel column with ethyl acetate–$CHCl_3$ mixtures (v/v, 0 : 100 → 70 : 30) used for elusion to afford **1** (4.4 mg), **12** (5.5 mg), and **7** (2.5 mg). Subfraction **K6** (857.7 mg) was chromatographed over a silica gel column with acetone–*n*-hexane gradient mixtures (v/v, 0 : 100 → 100 : 0) used for elution to give six subfractions (**K6.1–K6.6**). Subfraction **K6.3** (226.9 mg) was passed over a silica gel column, by elution with acetone–*n*-hexane gradient mixtures (v/v, 0 : 100 → 100 : 0), to obtain **13** (3.1 mg), while subfraction **K6.4** (301.5 mg) was purified by column chromatography with acetone–*n*-hexane gradient mixtures (v/v, 0 : 100 → 100 : 0), to afford **8** (4.9 mg). Subfraction **K6.6** (72.8 mg) was separated by chromatography over a silica gel column, by elution with ethyl acetate–*n*-hexane gradient mixtures (v/v, 0 : 100 → 100 : 0) and then the resulting fractions were purified by preparative TLC with isopropanol–ethyl acetate–$CHCl_3$ (v/v, 2 : 8 : 90), to furnish **2** (2.6 mg) and **9** (2.4 mg).

Calaburone A (1). Yellowish amorphous solid; IR (KBr) ν_{max} (cm^{-1}): 3458, 2925, 2855, 1737, 1637, 1509, 1459, 1366, 1213, 1104, 1036, 702; HR-ESI-MS *m*/*z* 329.1035 $[M + H]^+$ (calcd for $C_{18}H_{17}O_6^+$, 329.1025); ^1H NMR (CD_3COCD_3, 500 MHz) and ^{13}C NMR (CD_3COCD_3, 125 MHz) data are shown in Table 1 (Fig. S1–S9†).

Calaburone B (2). Yellowish amorphous solid; IR (KBr) ν_{max} (cm^{-1}): 3358, 2928, 2854, 1723, 1626, 1595, 1510, 1454, 1432, 1377, 1353, 1243 1208, 1170, 1107, 1038, 999, 825, 752; HR-ESI-MS *m*/*z* 345.0990 $[M + H]^+$ (calcd for $C_{18}H_{17}O_7^+$, 345.0974); ^1H NMR (CD_3COCD_3, 500 MHz) and ^{13}C NMR (CD_3COCD_3, 125 MHz) data are shown in Table 1 (Fig. S10–S16†).

Calaburone C (3). Yellowish amorphous solid; IR (KBr) ν_{max} (cm^{-1}): 3420, 2928, 2856, 1648, 1599, 1514, 1455, 1314, 1236, 1164, 1081, 1022, 932, 877, 797; HR-ESI-MS *m*/*z* 331.0820 $[M + H]^+$ (calcd for $C_{17}H_{15}O_7^+$, 331.0812); ^1H NMR (CD_3COCD_3, 500 MHz) and ^{13}C NMR (CD_3COCD_3, 125 MHz) data are shown in Table 1 (Fig. S17–S23†).

7-Hydroxyflavone (4). Yellowish amorphous solid; HR-ESI-MS *m*/*z* 239.0685 $[M + H]^+$ (calcd for $C_{15}H_{11}O_3^+$, 239.0703); ^1H NMR (CD_3COCD_3, 500 MHz) and ^{13}C NMR (CD_3COCD_3, 125 MHz) data are shown in ESI (Fig. S24–S26).†

7-Hydroxy-8-methoxyflavone (5). Yellowish amorphous solid; HR-ESI-MS *m*/*z* 269.0801 $[M + H]^+$ (calcd for $C_{16}H_{13}O_4^+$, 269.0809); ^1H NMR ($CDCl_3$, 500 MHz) and ^{13}C NMR ($CDCl_3$, 125 MHz) data are shown in ESI (Fig. S27–S29).†

3,7-Dimethoxyflavone (6). Yellowish amorphous solid; HR-ESI-MS *m*/*z* 283.0969 $[M + H]^+$ (calcd for $C_{17}H_{15}O_4^+$, 283.0965); ^1H NMR ($CDCl_3$, 500 MHz) and ^{13}C NMR ($CDCl_3$, 125 MHz) data are shown in ESI (Fig. S30–S32).†

5,7-Dimethoxy-6-hydroxyflavone (7). Yellowish amorphous solid; HR-ESI-MS *m*/*z* 299.0924 $[M + H]^+$ (calcd for $C_{17}H_{15}O_5^+$, 299.0914); ^1H NMR (CD_3COCD_3, 500 MHz) and ^{13}C NMR (CD_3COCD_3, 125 MHz) data are shown in ESI (Fig. S33–S35).†

Kaempferol (8). Yellowish amorphous solid; HR-ESI-MS *m*/*z* 287.0565 $[M + H]^+$ (calcd for $C_{15}H_{11}O_6^+$, 287.0550); ^1H NMR (CD_3COCD_3, 500 MHz) and ^{13}C NMR (CD_3COCD_3, 125 MHz) data are shown in ESI (Fig. S36–S38).†

4′-Hydroxywogonin (9). Yellowish amorphous solid; HR-ESI-MS *m*/*z* 301.0748 $[M + H]^+$ (calcd for $C_{16}H_{13}O_6^+$, 301.0707); ^1H NMR (CD_3COCD_3, 500 MHz) and ^{13}C NMR (CD_3COCD_3, 125 MHz) data are shown in ESI (Fig. S39–S41).†

6,7-Dimethoxy-5,4′-dihydroxyflavone (10). Yellowish amorphous solid; HR-ESI-MS *m*/*z* 315.0842 $[M + H]^+$ (calcd for $C_{17}H_{15}O_6^+$, 315.0863); ^1H NMR (CD_3COCD_3, 500 MHz) and ^{13}C NMR (CD_3COCD_3, 125 MHz) data are shown in ESI (Fig. S42–S44).†

5-Hydroxy-7,4′-dimethoxyflavone (11). Yellowish amorphous solid; HR-ESI-MS *m*/*z* 299.0934 $[M + H]^+$ (calcd for $C_{17}H_{15}O_5^+$, 299.0914); ^1H NMR ($CDCl_3$, 500 MHz) and ^{13}C NMR ($CDCl_3$, 125 MHz) data are shown in ESI (Fig. S45–S47).†

7-Hydroxy-4′-methoxyflavone (12). Yellowish amorphous solid; HR-ESI-MS *m*/*z* 269.0829 $[M + H]^+$ (calcd for $C_{16}H_{13}O_4^+$, 269.0809); ^1H NMR (CD_3COCD_3, 500 MHz) and ^{13}C NMR (CD_3COCD_3, 125 MHz) data are shown in ESI (Fig. S48–S50).†

Quercetin 3,7-dimethyl ether (13). Yellowish amorphous solid; HR-ESI-MS *m*/*z* 331.0794 $[M + H]^+$ (calcd for $C_{17}H_{15}O_7^+$, 331.0813); ^1H NMR (CD_3COCD_3, 500 MHz) and ^{13}C NMR (CD_3COCD_3, 125 MHz) data are shown in ESI (Fig. S51–S53).†

Quercetin 3,3′-dimethyl ether (14). Yellowish amorphous solid; HR-ESI-MS *m*/*z* 331.0842 $[M + H]^+$ (calcd for $C_{17}H_{15}O_7^+$, 331.0813); ^1H NMR (CD_3COCD_3, 500 MHz) and ^{13}C NMR (CD_3COCD_3, 125 MHz) data are shown in ESI (Fig. S54–S56).†

5,7,4′-Trihydroxy-3,8-dimethoxyflavone (15). Yellowish amorphous solid; HR-ESI-MS *m*/*z* 331.0805 $[M + H]^+$ (calcd for $C_{17}H_{15}O_7^+$, 331.0813); ^1H NMR (CD_3COCD_3, 500 MHz) and ^{13}C NMR (CD_3COCD_3, 125 MHz) data are shown in ESI (Fig. S57–S59).†

α-Glucosidase inhibitory assay

All crude extracts and isolated compounds were first dissolved in 0.01 M phosphate buffer (pH 7.0) and tested at concentrations between 1 and 250 μM. The reaction was initiated by mixing a solution containing 1.5 mM *p*-nitrophenyl-α-D-glucopyranoside (50 μL) and 0.1 U mL^{-1} α-glucosidase (50 μL) in 0.01 M phosphate buffer (pH 7.0) with the sample solution (525 μL). Reactions were carried out at 37 °C for 30 minutes and then halted by adding 0.1 M Na_2CO_3 (375 μL). Enzymatic activity was assessed by measuring absorbance at 401 nm using a Shimadzu UV-1800 spectrophotometer. The inhibition percentage (*I*%) was calculated with the following equation: $I\% = [(A_{control} - A_{sample})/A_{control}] \times 100\%$. Results were expressed as mean ±

standard error ($n = 3$). IC_{50} values were calculated using the software. Acarbose served as a positive control.

Molecular docking and molecular dynamics simulation

Molecular docking was performed on the complexes of the α-glucosidase (PDB ID: 3A4A) and compound **3**, **14**, and **15**. The workflow were as follows: SMILES formats of all ligands were converted into 3D formats using the OpenBabel utility. Prior to docking, protein and compound structures were prepared by eliminating all non-standard residues, incorporating missing hydrogen atoms, and assigning charges *via* the Dock Prep tool in UCSF Chimera (version 1.17.3). Docking procedures were then performed with AutoDock Vina (version 1.1.2). Molecular docking on α-glucosidase was conducted at active site with the docking box configuration as 35.20 Å × 27.12 Å × 30.7 Å with centre coordinates at $x = 19.23$, $y = -10.14$, and $z = 24$. PyMOL 3.0 software was employed to visualize 3D docking poses, while Biovia Discovery Studio 21.1 was used to illustrate 2D interactions between the enzyme and the compounds.

Molecular dynamics (MD) simulations were carried out on the native α-glucosidase and its docked complexes with the ligands using GROMACS 2024.1. The topology of α-glucosidase was generated with the CHARMS-36 force field and TIP3P GROMACS recommended water model. Ligand topologies were prepared using CGENFF web server tool and then converted to GROMACS compatible file using a Python script provided by the Mackerell lab. The topology files for α-glucosidase and ligands were manually merged using text editor. Next, the system was then enclosed in a dodecahedron box with a minimum distance of 1 nm between the system and the box wall. Solvation was performed using the SPC216 explicit water model, followed by neutralization with 20 Na^+ ions. Energy minimization was conducted using the steepest descent algorithm until atomic forces dropped below 100 kJ mol^{-1} nm^{-1}. Equilibration was performed in two phases under position restraints, each with a 2 fs time step and a duration of 1 ns. The first phase used an *NVT* ensemble with a V-rescale thermostat at 300 K, while the second phase employed an *NPT* ensemble with a C-rescale barostat at 1 bar. The Particle Mesh Ewald (PME) method handled long-range electrostatics, and a 1 nm cutoff was applied to short-range electrostatics and van der Waals interactions. The LINCS algorithm constrained hydrogen bonds during equilibration and production runs. Finally, a 100 ns production simulation was conducted with trajectory snapshots saved every 10 ps.

The free binding energies between protein and ligands were calculated using the Molecular Mechanics/Poisson–Boltzmann Surface Area (MMPBSA) method with gmx_MMPBSA v1.5.1.[40,41] For this analysis, 800 frames were extracted from the final 40 ns of each molecular dynamics (MD) trajectory. The ligand binding free energy (ΔTOTAL) was determined by subtracting the free energies of the receptor and ligand from that of the complex. The total free energy for each system was the sum of gas-phase energy (GGAS) and solvation energy (GSOLV). GGAS was primarily composed of van der Waals (VDWAALS) and electrostatic (EEL) interactions, while GSOLV included contributions from polar (EPB) and nonpolar (ENPOLAR) interactions.

Abbreviations

AGIs	α-Glucosidase inhibitors
COSY	Correlation spectroscopy
d	Doublet
dt	Doublet of triplet
DEPT	Distortionless enhancement by polarization transfer
EEL	Electrostatic
ENPOLAR	Nonpolar
EPB	Polar
GGAS	Gas-phase energy
GSOLV	Solvation energy
HMBC	Heteronuclear multiple bond correlation
HSQC	Heteronuclear single quantum correlation
HR-ESI-MS	High-resolution electrospray ionization mass spectrometry
IC_{50}	Half-maximum inhibitory concentration
IR	Infrared
J	Coupling constant
m	Multiplet
MD	Molecular dynamics
MMPBSA	Molecular mechanics/Poisson–Boltzmann surface area
NMR	Nuclear magnetic resonance
NOESY	Nuclear Overhauser effect spectroscopy
PME	Particle mesh Ewald
RMSD	Root mean square deviation
RMSF	Root mean square fluctuation
s	Singlet
SAR	Structure–activity relationship
t	Triplet
T2DM	Type 2 diabetes mellitus
TLC	Preparative thin-layer chromatography
VDWAALS	van der Waals

Data availability

The primary data supporting this work are included in the ESI.†

Author contributions

The manuscript was written through the contributions of all authors. All authors have approved the final version of the manuscript.

Conflicts of interest

There are no conflicts to declare.

Acknowledgements

This research is funded by Vietnam National University, Ho Chi Minh City (VNU-HCM) under grant number 562-2022-18-04.

References

1 S. H. Min, J. H. Yoon, S. Hahn and Y. M. Cho, *J. Diabetes Invest.*, 2018, **9**, 893–902.
2 X. Zhang, L. Xu, H. Chen, X. Zhang, Y. Lei, W. Liu, H. Xu, B. Ma and C. Zhu, *J. Med. Chem.*, 2022, **65**, 9174–9192.
3 P. H. Dang, H. X. Nguyen, H. H. T. Nguyen, T. D. Vo, T. H. Le, T. H. N. Phan, M. T. T. Nguyen and N. T. Nguyen, *J. Nat. Prod.*, 2017, **80**, 1876–1882.
4 M. Singh, M. Kaur and O. Silakari, *Eur. J. Med. Chem.*, 2014, **84**, 206–239.
5 Y. Li, J. Yao, C. Han, J. Yang, M. T. Chaudhry, S. Wang, H. Liu and Y. Yin, *Nutrients*, 2016, **8**, 167.
6 R. Naskar, A. Ghosh, R. Bhattacharya and S. Chakraborty, *Neurochem. Int.*, 2024, 105859.
7 D. Sohretoglu and S. Sari, *Phytochem. Rev.*, 2020, **19**, 1081–1092.
8 C. Proenca, M. Freitas, D. Ribeiro, E. F. T. Oliveira, J. L. C. Sousa, S. M. Tome, M. J. Ramos, A. M. S. Silva, P. A. Fernandes and E. Fernandes, *J. Enzyme Inhib. Med. Chem.*, 2017, **32**, 1216–1228.
9 H. Cao and X. Chen, *Anticancer Agents Med. Chem.*, 2012, **12**, 929–939.
10 H. Tang, L. Huang, C. Sun and D. Zhao, *Food Funct.*, 2020, **11**, 3332–3350.
11 O. Abchir, M. Khedraoui, I. Yamari, H. Nour, A. Errougui, A. Samadi and S. Chtita, *PLoS One*, 2024, **19**, e0308308.
12 F. Rizvi, R. Ahmed, M. A. Bashir, S. Ullah, H. Zafar, W. Atia Tul, H. Siddiqui and M. I. Choudhary, *Future Med. Chem.*, 2023, **15**, 1757–1772.
13 M. Kwon, S. K. Ko, M. Jang, G. H. Kim, I. J. Ryoo, S. Son, H. W. Ryu, S. R. Oh, W. K. Lee, B. Y. Kim, J. H. Jang and J. S. Ahn, *J. Enzyme Inhib. Med. Chem.*, 2019, **34**, 1481–1488.
14 N. D. Mahmood, N. L. Nasir, M. S. Rofiee, S. F. Tohid, S. M. Ching, L. K. Teh, M. Z. Salleh and Z. A. Zakaria, *Pharm. Biol.*, 2014, **52**, 1598–1623.
15 J. J. Chen, H. H. Lee, C. D. Shih, C. H. Liao, I. S. Chen and T. H. Chou, *Planta Med.*, 2007, **73**, 572–577.
16 W. L. Kuo, H. R. Liao and J. J. Chen, *Molecules*, 2014, **19**, 20521–20535.
17 A. S. Sufian, K. Ramasamy, N. Ahmat, Z. A. Zakaria and M. I. M. Yusof, *J. Ethnopharmacol.*, 2013, **146**, 198–204.
18 H. T. Le, T. T. T. Tran, T. N. Van Do, H. X. Nguyen, P. T. Le, T. A. Nguyen and M. T. T. Nguyen, *Sci. Technol. Dev. J. Natl. Sci.*, 2022, **6**, 1856–1863.
19 T. H. Le, H. X. Nguyen, T. N. Van Do and M. T. T. Nguyen, *Vietnam J. Chem.*, 2023, **61**, 14–19.
20 T. N. Van Do, T. H. Le, H. X. Nguyen, T. N. T. Vo, P. H. Dang, N. T. Nguyen and M. T. T. Nguyen, *Nat. Prod. Res.*, 2022, **36**, 5524–5529.
21 Z. A. Zakaria, S. Mustapha, M. R. Sulaiman, A. M. Mat Jais, M. N. Somchit and F. C. Abdullah, *Med. Princ. Pract.*, 2007, **16**, 130–136.
22 Z. A. Zakaria, M. R. Sulaiman, A. M. M. Jais, M. N. Somchit, K. V. Jayaraman, G. Balakhrisnan and F. C. Abdullah, *Fundam. Clin. Pharmacol.*, 2006, **20**, 365–372.
23 H. H. Math, R. S. Kumar, B. Chakraborty, A. I. Almansour, K. Perumal, G. B. Kantli and S. Nayaka, *Antibiotics*, 2023, **12**, 1175.
24 A. R. Saba, Doctor of Philosophy, Università degli Studi di Cagliari, 2012.
25 C. A. Kingsbury and J. H. Looker, *J. Org. Chem.*, 1975, **40**, 1120–1124.
26 M. Osorio-Olivares, B. K. Cassels, S. Sepúlveda-Boza and M. C. Rezende, *Synth. Commun.*, 1999, **29**, 815–819.
27 R. Singh, B. Singh, S. Singh, N. Kumar, S. Kumar and S. Arora, *Toxicol. In Vitro*, 2008, **22**, 1965–1970.
28 T. Tomimori, Y. Miyaichi, Y. Imoto, H. Kizu and T. Namba, *Chem. Pharm. Bull.*, 1986, **34**, 406–408.
29 M. Ghanadian, R. A. Jahanshahi, H. Fakhim, H. Yousefi, A. Matkowski, M. Khodadadi and S. Gharibi, *Res. Pharm. Sci.*, 2023, **18**, 317–325.
30 A. K. Bashir, *J. Herbs, Spices Med. Plants*, 1995, **3**, 17–24.
31 H. O. Yang, D.-Y. Suh and B. H. Han, *Planta Med.*, 1995, **61**, 37–40.
32 Y. Park, B. H. Moon, H. Yang, Y. Lee, E. Lee and Y. Lim, *Magn. Reson. Chem.*, 2007, **45**, 1072–1075.
33 M. Guerrero, P. Puebla, R. Carrón, M. Martin and L. S. Román, *J. Pharm. Pharmacol.*, 2002, **54**, 1373–1378.
34 J. Wu, Z. Wan, Y. Wu, W. Peng, C. Zheng and J. Wu, *Chem. Nat. Compd.*, 2013, **49**, 759–760.
35 J. N. Roitman and L. F. James, *Phytochemistry*, 1985, **24**, 835–848.
36 C. Proença, M. Freitas, D. Ribeiro, E. F. T. Oliveira, J. L. C. Sousa, S. M. Tomé, M. J. Ramos, A. M. S. Silva, P. A. Fernandes and E. Fernandes, *J. Enzyme Inhib. Med. Chem.*, 2017, **32**(1), 1216–1228.
37 F. A. Van de Laar, P. L. Lucassen, R. P. Akkermans, E. H. Van de Lisdonk, G. E. Rutten and C. Van Weel, *Cochrane Database Syst. Rev.*, 2005, **2005**(2), CD003639.
38 K. Yamamoto, H. Miyake, M. Kusunoki and S. Osaki, *FEBS J.*, 2010, **277**, 4205–4214.
39 Z. Moosavi-Movahedi, N. Salehi, M. Habibi-Rezaei, F. Qassemi and M. H. Karimi-Jafari, *J. Mol. Graphics Modell.*, 2023, **122**, 108495.
40 M. S. Valdés-Tresanco, M. E. Valdés-Tresanco, P. A. Valiente and E. Moreno, *J. Chem. Theory Comput.*, 2021, **17**, 6281–6291.
41 B. R. Miller III, T. D. McGee Jr., J. M. Swails, N. Homeyer, H. Gohlke and A. E. Roitberg, *J. Chem. Theory Comput.*, 2012, **8**, 3314–3321.